

## Effect of the doubly magic shell closures in $^{132}\text{Sn}$ and $^{208}\text{Pb}$ on the mass distributions of fission fragments of superheavy nuclei


C. Ishizuka<sup>1,\*</sup>, X. Zhang<sup>1,†</sup>, M. D. Usang<sup>2,‡</sup>, F. A. Ivanyuk<sup>1,3,§</sup> and S. Chiba<sup>1,4,||</sup>

<sup>1</sup>*Tokyo Institute of Technology, Tokyo, 152-8550 Japan*

<sup>2</sup>*Malaysia Nuclear Agency, Bangi, Malaysia*

<sup>3</sup>*Institute for Nuclear Research, 03028 Kiev, Ukraine*

<sup>4</sup>*National Astronomical Observatory of Japan, Tokyo, Japan*

 (Received 18 November 2019; revised manuscript received 17 December 2019; published 27 January 2020)

In this Rapid Communication, we try to settle down the controversial predictions on the effect of doubly magic nuclei  $^{132}\text{Sn}$  and  $^{208}\text{Pb}$  on the mass distributions of fission fragments of superheavy nuclei. For this, we have calculated the mass distribution of fission fragments of superheavy nuclei from  $^{274}\text{Hs}$  to  $^{306}122$  within the dynamical four-dimensional Langevin approach. We have found that, in “light” superheavies, the influence of  $^{208}\text{Pb}$  on the mass distributions is negligibly small. In “heavy” superheavies,  $Z = 120\text{--}122$ , the (quasi)symmetric peaks and strongly asymmetric peaks at fragment mass  $A_F$  close to  $A_F = 208$  are of comparable magnitude to  $A_F = 132\text{--}140$ .

DOI: [10.1103/PhysRevC.101.011601](https://doi.org/10.1103/PhysRevC.101.011601)

**Introduction.** The physics of superheavy elements (SHEs) has a long history. The existence of the “island of stability”—the region of nuclei with the increased stability with respect to spontaneous fission—was predicted at the middle of the 1960s. The possibility of closed shells at  $Z = 114$ ,  $N = 184$  was pointed out already in Refs. [1–3]. The systematic calculations in Ref. [4] within the macroscopic-microscopic method [5–7] for SHEs with the number of protons  $106 < Z < 116$  have shown that many superheavies are very stable with the spontaneous fission half-lives of thousands of years or more. The highest fission barrier was predicted for a new double magic nucleus with  $Z = 114$  and  $N = 184$ . Nevertheless, it took almost 30 years until the  $\alpha$  decay of the element with  $Z = 114$  was observed experimentally at Flerov Laboratory for Nuclear Reactions in Dubna [8]. During the next two decades, a lot of new experimental achievements were synthesized. The theoretical works were dedicated to the search of the most favorable pairs of the projectile and target and the excitation energy that would lead to the largest cross section of the formation of evaporation residue—the superheavy nucleus in its ground state.

With the development of the experimental facility, it became possible not only to fix the fact of formation of the SHE, but also to accumulate so many superheavy nuclei that it turned out possible to examine their properties. One of the first properties of interest—the process of fission of SHEs. For the successful planning and carrying out of experiments, it is

very important to understand what kind of fission fragments one should expect in the result of fission of the SHE. On one side, it is clear that, with increasing charge number  $Z$  of the fissioning nucleus, the Coulomb repulsion force grows and one could expect the symmetric mass distribution of fission fragments. On the other side—the shell effects may still have a noticeable effect. The two double magic nuclei may contribute. The  $^{132}\text{Sn}$  and  $^{208}\text{Pb}$  have the shell correction to the ground-state energy of the same magnitude. The  $^{132}\text{Sn}$  plays a decisive role in the formation of mass distribution of actinide and transactinide nuclei. In the experiment of the Itkis group [9,10],  $^{132}\text{Sn}$  was found out as the light fragment of all investigated nuclei. The theoretical calculation within the scission point model [11] also predicts  $^{132}\text{Sn}$  (or slightly heavier) as the most probably light fragment for the fission of the SHE. At the same time, there are few publications [12–15] where the formation of a heavy fragment close to  $^{208}\text{Pb}$  is predicted as a main fission mode. In Ref. [16], the heavy fragment close to  $^{208}\text{Pb}$  was obtained in the superheavy region  $106 < Z < 114$ .

In order to solve this contradiction and make it clear what kind of fission fragment mass distribution (FFMD) one could expect in the fission of SHEs, we have carried out the calculations of the FFMD for a number of SHEs within the four-dimensional Langevin approach. We have found out the  $^{208}\text{Pb}$  may appear as a supplementary heavy cluster in the fission of Cn isotopes. With an increasing charge number of SHEs, the contribution of this heavy cluster became larger. For the element with  $Z = 122$ , the contributions of (almost) symmetric and strongly mass asymmetric ( $A_F \approx 208$ ) are of the same magnitude. The details of calculations are given below.

**The model.** We describe the fission process within the Langevin approach [17], i.e., by solving the equations for

\*chikako@nr.titech.ac.jp

†zhang.x.ba@m.titech.ac.jp

‡mark\_dennis@nuclearmalaysia.gov.my

§ivanyuk@kinr.kiev.ua

||chiba.satoshi@nr.titech.ac.jp

the time evolution of the shape of the nuclear surface of the fissioning system. For the shape parametrization, we use that of the two-center shell model (TCSM) [18] with four deformation parameters  $q_\mu = z_0/R_0, \delta_1, \delta_2, \alpha$ . Here,  $z_0/R_0$  refers to the distance between the centers of the left and right oscillator potentials with  $R_0 = 1.2A^{1/3}$ ,  $R_0$  being the radius of the spherical nucleus with the mass number  $A$ . The parameters  $\delta_i$ , where  $i = 1, 2$  describe the deformation of the right and left fragment tips. The fourth parameter  $\alpha$  is the mass asymmetry, and the fifth parameter of TCSM shape parametrization  $\epsilon$  was kept constant at  $\epsilon = 0.35$  in all our calculations.

The first-order differential equations (Langevin equations) for the time dependence of collective variables  $q_\mu$  and the conjugated momenta  $p_\mu$  are as follows:

$$\begin{aligned} \frac{dq_\mu}{dt} &= (m^{-1})_{\mu\nu} p_\nu, \\ \frac{dp_\mu}{dt} &= -\frac{\partial F(q, T)}{\partial q_\mu} - \frac{1}{2} \frac{\partial (m^{-1})_{\nu\sigma}}{\partial q_\mu} p_\nu p_\sigma \\ &\quad - \gamma_{\mu\nu} (m^{-1})_{\nu\sigma} p_\sigma + g_{\mu\nu} R_\nu(t), \end{aligned} \quad (1)$$

$$(2)$$

where the sums over the repeated indices are assumed. In Eqs. (1) and (2) the  $F(q, T)$  is the temperature-dependent free energy of the system,  $\gamma_{\mu\nu}$  and  $(m^{-1})_{\mu\nu}$  are the friction and the inverse of mass tensors, and  $g_{\mu\nu}$  is the random force.

The free-energy  $F(q, T)$  is calculated as the sum of liquid drop deformation energy and the temperature-dependent shell correction  $\delta F(q, T)$ . The damping of shell correction  $\delta F(q, T)$  with the excitation energy is described in detail in Ref. [19]. The single-particle energies are calculated with the deformed Woods-Saxon potential [20,21] fitted to the aforementioned TCSM shape parametrizations. It is to be noted that the free energy is equal to the potential energy at zero temperature.

The collective inertia tensor  $m_{\mu\nu}$  is calculated within the Werner-Wheeler approximation [22], and for the friction tensor  $\gamma_{\mu\nu}$ , we used the wall-and-window formula [23,24].

The random force  $g_{\mu\nu} R_\nu(t)$  is the product of white-noise  $R_\nu(t)$  and the temperature-dependent strength factors  $g_{\mu\nu}$ . The factors  $g_{\mu\nu}$  are related to the temperature and friction tensor via the modified Einstein relation,

$$g_{\mu\sigma} g_{\sigma\nu} = T^* \gamma_{\mu\nu}, \quad \text{with } T^* = \frac{\hbar\omega}{2} \coth \frac{\hbar\omega}{2T},$$

where  $T^*$  is the effective temperature [25]. The parameter  $\omega$  is the local frequency of collective motion [25]. The minimum of  $T^*$  is given by  $\hbar\omega/2$ .

The temperature  $T$  in this context is related to the reaction energy  $E_x$  and the internal excitation energy  $E^*$  by

$$E^* = E_{\text{gs}} + E_x - \frac{1}{2} m_{\mu\nu}^{-1} p_\mu p_\nu - V_{\text{pot}}(q, T=0) = aT^2,$$

where  $V_{\text{pot}}$  is the potential energy and  $a$  is the level-density parameter. More details are given in our earlier publications, see Refs. [26–29]. Initially, the momenta  $p_\mu$  are set to be equal to zero, and calculations are started from the ground-state deformation. Such calculations are continued until the trajectories reach the “scission point,” which was defined as the point in deformation space where the neck radius reaches the value of  $r_{\text{neck}} = 1$  fm.

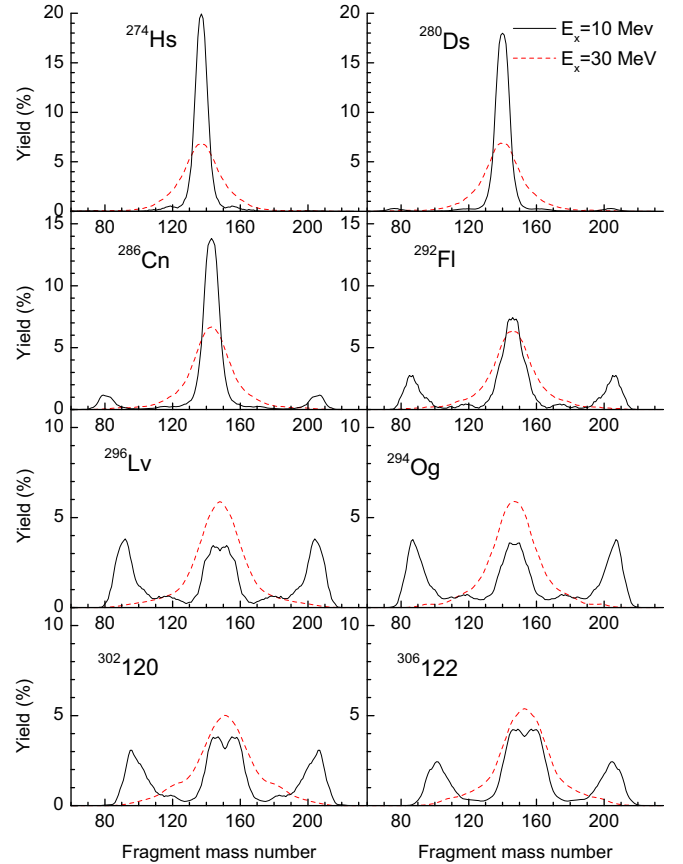


FIG. 1. The fission fragment mass distributions of superheavy nuclei from  $^{274}\text{Hs}$  to  $^{306}122$  calculated for the excitation energy  $E_x = 10$  and  $E_x = 30$  MeV as a function of fragment mass number.

*Numerical results.* In Fig. 1, we show the fission fragment mass distributions of superheavy nuclei from  $^{274}\text{Hs}$  to  $^{306}122$  as a function of fragment mass number  $A_F$ . As one can see, at  $E_x = 30$  MeV, the shell structure is washed out, and all considered here nuclei fission symmetrically. At excitation energy  $E_x = 10$  MeV, the lighter superheavies Hs and Ds also undergo mass symmetric fission. The FFMDs of nuclei from  $^{286}\text{Cn}$  to  $^{306}122$  have three or four peak structures. Obviously, the multippeak structures of the FFMDs are the result of shell effects, which, at  $E_x = 10$  MeV, are still large. The symmetric peak which, in heavier SHEs, is split into two components. The peaks of lighter fragments are located around  $A_F = 140$ .

One can also see the strongly asymmetric peak at the mass number close to  $A_F = 208$ . The strength of the (almost) symmetric and asymmetric components in the FFMD of the SHEs depends on the proton and neutron numbers of the compound nucleus. For  $^{286}\text{Cn}$ , the contribution of the strongly asymmetric peak is very small. This contribution becomes larger for heavier SHEs. In the element  $^{306}122$ , the symmetric and mass asymmetric peaks are of the same magnitude.

In order to understand the reason for such a complicated structure, we have looked at the potential energy of fissioning nuclei. Figure 2 shows the potential energy  $E_{\text{def}}$  of the nucleus with  $Z = 120$  and  $A = 302$  at zero temperature as the function

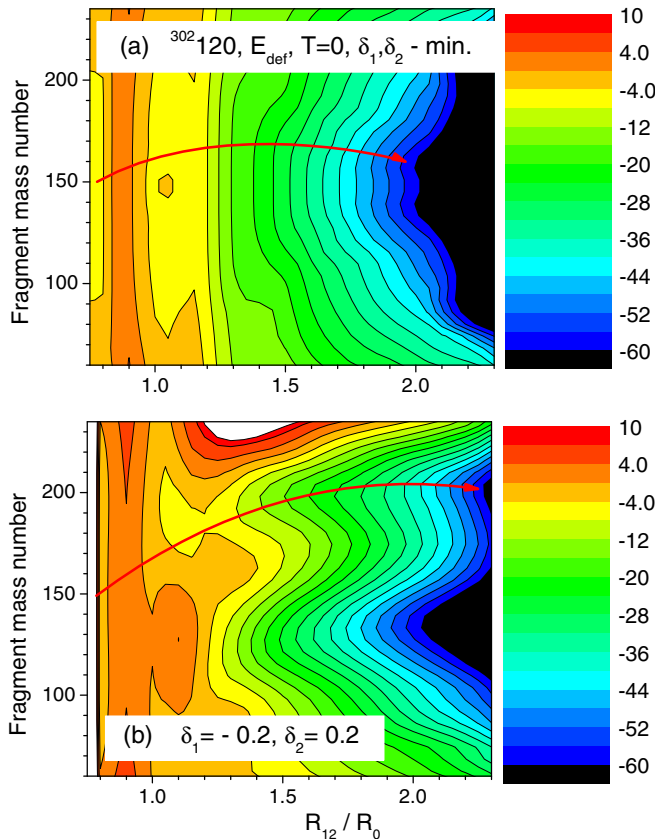


FIG. 2. (a) The potential energy of  $^{302}\text{120}$  at  $T = 0$  minimized with respect to deformation parameters  $\delta_1$  and  $\delta_2$ . (b) The potential energy of  $^{302}\text{120}$  at  $T = 0$  at fixed values of  $\delta_1 = -0.2$  and  $\delta_2 = 0.2$ .

of elongation (the distance  $R_{12}$  between left and right parts of the nucleus) and mass asymmetry. In Fig. 2(a), the energy was minimized with respect to the deformation parameters  $\delta_1$  and  $\delta_2$ . One clearly sees the bottom of the potential energy leading to almost symmetric mass splitting. There is also a hint on the mass asymmetric valley at  $A_F$  close to  $A_F = 208$ . If the trajectories would follow the bottom of the potential energy, then the mass FFMD of  $^{302}\text{120}$  would be mass symmetric. However, it is well known that due to dynamical effects the trajectories may deviate substantially from the bottom of the potential valley. We calculate the trajectories in four-dimensional deformation space. In this space, there could be the local minima leading away from the bottom of the potential valley. An example is shown in Fig. 2(b). Here, we show the potential energy for fixed  $\delta_1 = -0.2$  and  $\delta_2 = 0.2$ .

One can see that in this subspace the trajectories can easily be trapped in the higher energy valley leading to highly asymmetric fission. The trajectories cannot skip into a deeper symmetric valley because of the barrier between these two valleys. In this way, the strongly mass asymmetric peak appears in the mass distribution of the fission fragments. In order to understand why these effects get stronger for heavier SHEs, we have compared the dependence of the potential energy close to the scission point at  $R_{12}/R_0 = 2.3$  on the mass asymmetry for two nuclei  $^{286}\text{Cn}$  and  $^{306}\text{122}$ , see Fig. 3.

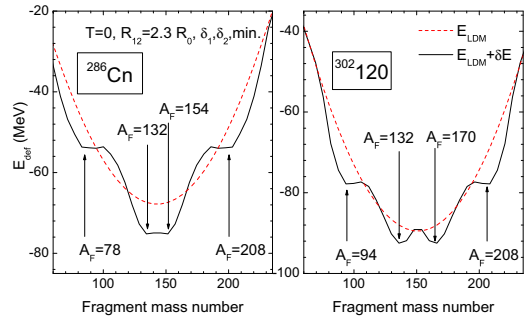


FIG. 3. The liquid drop (dashed curves) and the total (solid curves) deformation energies near the scission line ( $R_{12} = 2.3R_0$ ) for  $^{286}\text{Cn}$  and  $^{302}\text{120}$  as a function of fragment mass number.

In Fig. 3, we compare the total deformation energies near the scission line for  $^{286}\text{Cn}$  and  $^{302}\text{120}$  with those of the liquid drop model. One can see that in the case of  $^{286}\text{Cn}$ , the local minima corresponding to  $A_F = 208$  and its paired fission fragment  $A_F = 78$  are by 20 MeV higher than the minimum around  $A_F = 132-154$ . For  $^{306}\text{122}$ , the difference in almost symmetric, and strongly mass asymmetric minima is smaller by only 14 MeV. Thus, in this case, the trajectories have more chances to get into the mass asymmetric valley at  $A_F = 208$  and its pair  $A_F = 94$ . As a result, the obtained FFMD becomes double mass asymmetric as seen in Fig. 1.

Another reason for the appearing of the  $A_F = 208$  contribution is the  $Z/A$  ratio. The  $Z/A$  ratio of the fission fragment and of the mother nucleus is approximately the same. For  $^{132}\text{Sn}$ , this factor is equal to 0.379, whereas for  $^{208}\text{Pb}$ , this ratio is equal to 0.394. The last ratio is much closer to that of  $^{286}\text{Cn}$  and  $^{306}\text{122}$  which are equal to 0.392 and 0.397 correspondingly.

In Fig. 4, we investigate the quadrupole deformation  $Q_{20}$  of the fragments  $Q_{20} = \langle r^2 Y_{20}(\cos \theta) \rangle$  from  $^{236}\text{U}$  to  $^{306}\text{122}$ . The  $Q_{20}$  is the main measure of the deformation of the fragment's shape. The negative  $Q_{20}$  corresponds to the oblate shape, the shape is spherical at  $Q_{20} = 0$ , and positive  $Q_{20}$  corresponds to the prolate shape. In actinides from  $^{236}\text{U}$  to  $^{259}\text{Lr}$ , there is no sign of a  $^{208}\text{Pb}$  shell. On the other hand, in SHEs from  $^{274}\text{Hs}$  to  $^{306}\text{122}$ , one can clearly observe the  $Q_{20}(A)$  distributions located in both  $A_F = 132$  and 208, although we hardly see the peak at  $A_F = 208$  of  $^{274}\text{Hs}$  in the mass distribution shown in Fig. 1. Note that the averaged  $Q_{20}$  in actinides from  $^{236}\text{U}$  to  $^{257}\text{Fm}$  have positive  $Q_{20}$  in common, whereas the averaged  $Q_{20}$  in actinides from  $^{258}\text{Fm}$  to  $^{259}\text{Lr}$  commonly have  $Q_{20} \simeq 0$ . It means that the deformed shell around  $A_F = 132-140$  dominates the nuclear fission of actinides up to  $^{257}\text{Fm}$ , although the spherical  $^{132}\text{Sn}$  strongly affects the fission of actinides at and above  $^{258}\text{Fm}$ . In the same way, in the SHEs, we found that the fragments with mass number  $A_F = 132-140$  are both deformed and of spherical shape with  $Q_{20} \geq 0$ , the fragments with  $A_F = 208$ , are spherical with  $Q_{20} \approx 0$ . In this manner, we can demonstrate that two spherical magicities at  $A = 132$  and 208 play decisive roles in fission mechanisms.

Such results are quite reasonable because these fragments are nuclei with the double-closed shells. Another notable feature of  $Q_{20}(A_F)$  plots is the difference of the distribution

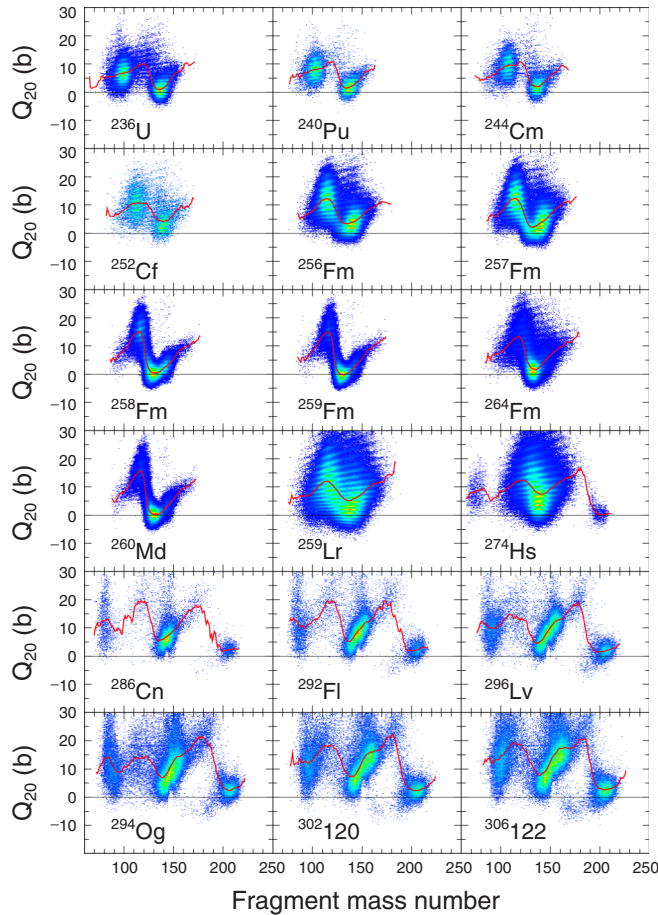


FIG. 4. The distribution of quadrupole deformation  $Q_{20}$  with respect to fission fragment mass number for nuclei from  $^{236}\text{U}$  to  $^{306}\text{122}$ . The red curves mark the average values of  $Q_{20}$ .

pattern between actinides ( $^{236}\text{U}$  to  $^{259}\text{Lr}$ ) and SHN ( $^{286}\text{Cn}$  to  $^{306}\text{122}$ ). The  $Q_{20}(A_F)$  distributions of actinides consist of two groups; the nearly spherical heavy fragments with  $A_F = 132\text{--}140$  and the prolate light fragments. For the superheavies from  $^{286}\text{Cn}$  to  $^{306}\text{122}$ , we observe the spherical heavier fragments with the mass number around  $A = 208$  and the complementary lighter fragments in addition to the mentioned above two groups seen in actinides.

In Ref. [29], we have noted a very accurate correlation between the dependence of the elongation of the fragment and the multiplicity of prompt neutrons—the number of neutrons per fission event emitted from completely accelerated fragments. So, the average values of  $Q_{20}$  (solid curves in Fig. 4) represent actually the mass dependence of neutron multiplicity, which is an important observable of the fission process.

It should be pointed out that, in the experiment by the Itkis group [9,10], they found a peak around  $A = 208$  and at complementary light mass numbers. However, these peaks were assigned to be formed by the quasifission process not by fusion-fission. Such an interpretation is natural since the composite systems formed by hot-fusion reactions have excitation energy, at least, around 30 MeV, and the subtle shell effect, which gives rise to the formation of the  $A = 208$  and complementary fragments, is washed out. Our calculation tells that only a small fraction of this peak can be, indeed, from fission of the compound nucleus (indicating the SHE was formed with slightly larger probability), but it is overwhelmed by the quasifission component, so it cannot be identified in experiments. The only possibility that this superasymmetric fusion-fission component can be observed is after emission of a few prescission neutrons to cool the residues to excitation energy region down to around 10 MeV. If, e.g., multiplicities of prescission neutrons and fission fragments from corresponding residues are observed in coincidence, there is a chance that this superasymmetric component to be identified to come from fusion-fission events. It is highly desirable to have an experimental setup to distinguish these two components, namely, quasifission and fusion-fission, forming the same peaks.

*Summary.* Within the four-dimensional Langevin approach, we have calculated the mass distributions of fission fragments of superheavy nuclei from  $^{274}\text{Hs}$  to  $^{306}\text{122}$ . We have found a three-four peak structure of mass distributions. In light superheavies, we see the dominant mass symmetric peak and small contributions from two highly asymmetric peaks at  $A_H \approx 208$  and at the supplementary light fragment mass  $A_L = A - 208$ . With increasing mass of fissioning nuclei the symmetric peak splits into two components and the strongly mass asymmetric peaks become higher. For  $^{306}\text{122}$ , all four peaks in FFMD are approximately of the same magnitude. So, in the fission process of superheavy nuclei, one would observe both the fragment with the mass number close to  $^{132}\text{Sn}$ ,  $A_F \approx 140$  plus the rest and the almost spherical fragment with the mass number  $A_F \approx 208$  plus the rest.

*Acknowledgments.* This Rapid Communication comprises the results of “Research and development of an innovative transmutation system of LLFP by fast reactors” entrusted to the Tokyo Institute of Technology by the Ministry of Education, Culture, Sports, Science and Technology of Japan (MEXT) and JSPS KAKENHI Grant Number 18K03642. One of us (F.A.I.) was supported, in part, by the Project “Fundamental research in high energy physics and nuclear physics” of the National Academy of Sciences of Ukraine. We appreciate very much the useful discussions with Prof. N. Carjan and Prof. A.V. Karpov.

- [1] W. D. Myers and W. J. Swiatecki, Lawrence Berkeley National Laboratory Report No. UCRL-11980, 1965 (unpublished).
- [2] A. Sobiczewski, F. A. Gareev, and B. N. Kalinkin, *Phys. Lett.* **22**, 500 (1966).
- [3] H. Meldner, *Ark. Fys.* **36**, 593 (1967).

- [4] S. G. Nilsson, C. F. Tsang, A. Sobiczewski *et al.*, *Nucl. Phys. A* **131**, 1 (1969).
- [5] W. D. Myers and W. J. Swiatecki, *Nucl. Phys.* **81**, 1 (1966).
- [6] V. M. Strutinsky, *Nucl. Phys. A* **95**, 420 (1967).
- [7] V. M. Strutinsky, *Nucl. Phys. A* **122**, 1 (1968).

- [8] Y. T. Oganessian, A. V. Yeremin, A. G. Popeko *et al.*, *Nature (London)* **400**, 242 (1999).
- [9] M. G. Itkis, A. A. Bogatchev, I. M. Itkis *et al.*, *J. Nucl. Rad. Sci.* **3**, 57 (2002).
- [10] M. G. Itkis, E. Vardaci, I. M. Itkis, G. N. Knyazheva, and E. V. Kozulin, *Nucl. Phys.* **A944**, 204 (2015).
- [11] N. Carjan, F. A. Ivanyuk, and Y. T. Oganessian, *Phys. Rev. C* **99**, 064606 (2019).
- [12] D. N. Poenaru and R. A. Gherghescu, *Phys. Rev. C* **97**, 044621 (2018).
- [13] M. Warda, A. Zdeb, and L. M. Robledo, *Phys. Rev. C* **98**, 041602(R) (2018).
- [14] Z. Matheson, S. A. Giuliani, W. Nazarewicz, J. Sadhukhan, and N. Schunck, *Phys. Rev. C* **99**, 041304(R) (2019).
- [15] G. Kaur and M. K. Sharma, *Nucl. Phys. A* **990**, 79 (2019).
- [16] M. Albertsson, B. G. Carlsson, T. Døssing, P. Möller, J. Randrup, and S. Åberg, [arXiv:1910.06030](https://arxiv.org/abs/1910.06030).
- [17] Y. Abe, S. Ayik, P.-G. Reinhard, and E. Suraud, *Phys. Rep.* **275**, 49 (1996).
- [18] J. Maruhn and W. Greiner, *Z. Phys.* **251**, 431 (1972).
- [19] F. A. Ivanyuk, C. Ishizuka, M. D. Usang, and S. Chiba, *Phys. Rev. C* **97**, 054331 (2018).
- [20] V. V. Pashkevich, *Nucl. Phys. A* **169**, 275 (1971).
- [21] V. V. Pashkevich, *Nucl. Phys. A* **477**, 1 (1988).
- [22] K. T. R. Davies, A. J. Sierk, and J. R. Nix, *Phys. Rev. C* **13**, 2385 (1976).
- [23] J. Blocki, Y. Boneh, J. R. Nix *et al.*, *Ann. Phys. (NY)* **113**, 330 (1978).
- [24] A. J. Sierk and J. R. Nix, *Phys. Rev. C* **21**, 982 (1980).
- [25] H. Hofmann and D. Kiderlen, *Int. J. Mod. Phys. E* **7**, 243 (1998).
- [26] M. D. Usang, F. A. Ivanyuk, C. Ishizuka, and S. Chiba, *Phys. Rev. C* **94**, 044602 (2016).
- [27] C. Ishizuka, M. D. Usang, F. A. Ivanyuk, J. A. Maruhn, K. Nishio, and S. Chiba, *Phys. Rev. C* **96**, 064616 (2017).
- [28] M. D. Usang, F. A. Ivanyuk, C. Ishizuka, and S. Chiba, *Phys. Rev. C* **96**, 064617 (2017).
- [29] M. D. Usang, F. A. Ivanyuk, C. Ishizuka, and S. Chiba, *Sci. Rep.* **9**, 1525 (2019).